International Journal on Magnetic Particle Imaging
Vol 8, No 1, Suppl 1, Article ID 2203052, 4 Pages

Infinite Science Publishing

Proceedings Article

Computational modeling of superferromagnetism in finite-length chains of superparamagnetic Iron Oxide tracers for use in super-resolution Magnetic Particle Imaging

Chinmoy Saayujya [a,*] · K. L. Barry Fung [b] · Quincy Huynh [a] · Caylin Colson [b] · Benjamin Fellows [c] · Prashant Chandrasekharan [c] · Steven M. Conolly [a,c]

[a] Department of Electrical Engineering and Computer Sciences, UC Berkeley, Berkeley, USA
[b] UC Berkeley-UCSF Graduate Group in Bioengineering, Berkeley/San Francisco, USA
[c] Department of Bioengineering, UC Berkeley, Berkeley, USA
*Corresponding author, email: chinmoy@berkeley.edu

Abstract

Magnetic Particle Imaging (MPI) is a novel tracer imaging modality that images the spatial distribution of superparamagnetic iron oxide nanoparticles (SPIOs), allowing for the sensitive and radiation-free imaging of labeled cells and targeted disease. Recent works have shown that at high concentrations, SPIOs display extremely sharp magnetic responses, resulting in 10-fold resolution and signal improvements. Dubbed superferromagnetic iron oxide particles (SFMIOs), these particles appear to interact with neighbours, effectively amplifying applied fields. This work performs a simulation of ensembles of linear chains of interacting SPIOs to elucidate SFMIO behavior and guide practical constraints in SFMIO synthesis. We show that working within certain physical constraints (chain length distributions and SPIO separation) preserves the improvements observed from SFMIOs.

I. Introduction

Magnetic Particle Imaging (MPI) is an emerging positive-contrast imaging modality that directly images superparamagnetic iron oxide (SPIO) tracers in the body [1]. Pre-clinical MPI has demonstrated micromolar sensitivity for tracking stem and white blood cells, as well as in the imaging of cancer, lung perfusion and abdominal bleeding [2–5]. MPI resolution is determined by the ratio of the SPIO saturation strength to the gradient field strength [1, 6, 7]. MPI already has excellent sensitivity and ideal contrast, linearity and penetration depth. The only significant weakness is poor spatial resolution, now about 1.5 mm in a mouse [8]. All MPI studies to date assume non-interacting SPIOs. Recently, Tay et al. experimented with interacting SPIOs to dramatically improve MPI resolution. They showed experimentally that high local concentrations of SPIO tracers showed order-of-magnitude improvements in both SNR and resolution [9]. These resolution improvements could allow for 10-fold reduction in scanner gradient field strength and thus a 100-fold reduction in cost. Several experiments support the hypothesis that the observed super-resolution behavior is due to the formation of SPIO particle chains [9, 10, 11]. We propose that these super-resolution chains of SPIOs exhibit "superferromagnetism," since superparamagnetism does not exhibit remanence or coercivity [10].

II. Methods

We consider an ensemble of linear chains, each consisting of N spherical, superparamagnetic single-domain particles (each of radius a_k) in the presence of an applied magnetic field. The SPIO chains are identical and independent, allowing ensemble averaging across the k^{th} SPIO in each chain. This averaging permits the use of a Langevin saturator model for each SPIO in the chain. Assuming the adiabatic dipole moment of each nodal SPIO is aligned (anti)parallel to the chain axis (the only possible equilibrium positions), the magnitude of the magnetization of the k^{th} SPIO in each chain, M_k, is given by

$$M_k = \rho\, m_0 \mathscr{L}\left(\frac{m_0 \mu_0 H_k}{k_B T}\right) \tag{1}$$

where ρ is the particle spatial density, m_0 the magnitude of the particle magnetic moment, T the absolute ambient temperature, and μ_0 and k_B the vacuum permeability and Boltzmann constants respectively. $\mathscr{L}(x) = (\tanh x)^{-1} - x^{-1}$ is the Langevin function and H_k is the local magnetic field strength at the k^{th} SPIO. Each nodal SPIO feels an identical applied field plus the local dipole field from neighboring SPIOs:

$$H_k = H_k^{\text{applied}} + \frac{1}{2\pi}\sum_{i\neq k}^{N} \frac{m_i}{\Delta_{ik}^3} \tag{2}$$

where Δ_{ij} is the center-to-center distance between the i^{th} and j^{th} SPIO in each chain. With the nondimensionalizations $\phi_k = M_k/(\rho\, m_0)$ and $\tilde{B} = \mu_0 H/(k_B T/m_0)$, we obtain a set of transcendental equations describing the time-varying polarization $\phi_k(t)$ of the k^{th} SPIO in each chain as a function of the time-varying applied magnetic flux density

$$\phi_k(t) = \mathscr{L}\left(\tilde{B}^{\text{applied}}(t) + \frac{2\chi a_k^3}{3}\sum_{i\neq k}^{N}\frac{\phi_i(t)}{\Delta_{ik}^3}\right) \tag{3}$$

Here, χ is the magnetic susceptibility of superparamagnetic iron oxide, defined as

$$\chi = \mu_0 \frac{n\, m_0}{k_B T/m_0} \equiv \mu_0 \frac{M_{\text{sat}}}{B_{\text{sat}}} \tag{4}$$

This formulation generates a system of k transcendental equations that describe positive feedback, which is consistent with the observed hysteresis. The system is iteratively solved until an energetically stable, self-consistent solution is obtained. The external applied field is then stepped, akin to a DC magnetometry study, to obtain the complete magnetization curve. Relevant system parameters can be easily altered to accommodate particles of varying physical and magnetic properties. In this study, we simulate chains wherein each nodal SPIO is identical and equally separated. This is done to elucidate the dependence of coercivity on chain length N and interparticle separation.

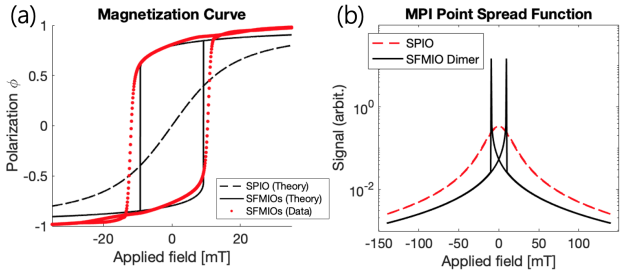

Figure 1: Simulated magnetization curve (a) shows hysteresis in SFMIO chains but not for non-interacting SPIOs [6]. There is good agreement between the SFMIO simulation and experiment. The derived MPI PSF (b) shows order-of-magnitude improvements in SFMIO resolution and signal over SPIOs.

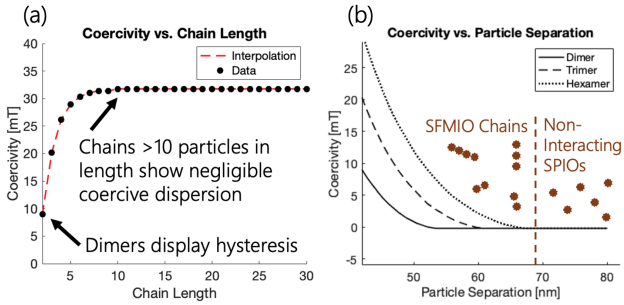

Figure 2: Parametric sweeps of chain length show coercivity increases monotonically with chain length (a). We observe negligible changes in coercivity beyond a certain chain length. Varying the inter-particle separation (b) shows that increasing this value beyond a certain point causes inter-particle interactions to vanish, resulting in regular SPIO behaviour.

III. Results

Adiabatic magnetization curves were generated for particles with a 20 nm diameter and 5 nm shell thickness (Figure 1(a)). We observe hysteresis in the magnetization curve for chains of ≥ 2 particles. The derived MPI point spread function (PSF) of the SFMIO chain in Figure 1(b) shows marked improvements in SNR (∼70-fold) and resolution (∼30-fold). Parametric sweeps in Figure 2(a) indicate that the coercive threshold does not vary with chain length above a certain size. Simulated data obtained by sweeping the applied field with a 1 kHz sinusoidal excitation (Figure 3) shows the odd harmonics necessary for MPI reconstruction [7].

IV. Discussion

The theoretical magnetization curves show good agreement with SFMIO data and can predict the coercive threshold. Deviations between theory and experiments are due to variations in particle size, coating thickness and chain length within the test sample. Experimental

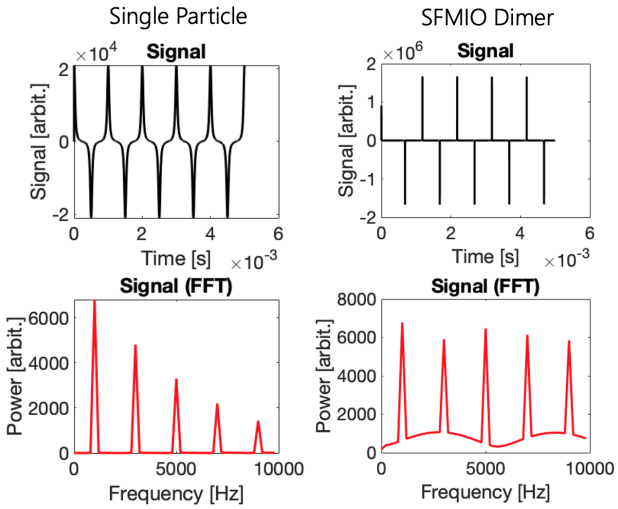

Figure 3: Subjecting the SFMIOs with a 1kHz sinusoidal excitation with sufficient amplitude to cause a coercive flip shows the full set of odd harmonics (bottom right) in the frequency spectrum, as necessary for MPI reconstruction. The raw signal shows an order-of-magnitude increase in the SFMIO signal (top right) over the SPIO signal (top left).

data also exhibits non-adiabatic relaxation effects in the coercive transition, which are unaccounted for.

Parametric sweeps indicate that the coercive threshold does not vary with chain length above a certain size, owing to the rapid spatial fall-off of the magnetic field away from each nodal dipole ($B(r) \propto 1/r^3$). This limits the maximum coercive dispersion (variance in the coercivity of chains with different lengths) allowing for generous practical tolerances in SFMIO chain synthesis. This is critical since a wide spread of coercivities within a tracer sample would result in significantly worse resolution as well as a marked increase in the complexity of MPI image reconstruction. Simulation shows that dimers also display hysteresis, paving the way for solely dimeric tracers with superior sensitivity and resolution but negligible magneto-motive drift, which could be a safety concern for longer chains.

We expect some resolution and SNR losses from particle relaxation. We can also account for coercivity dispersion by considering a distribution of chain lengths within the test sample, which will manifest as further PSF blurring. We find that coercivity is a monotonic function of SPIO shell thickness (Figure 2(b)), vanishing for very thick shells as expected.

V. Conclusion

We successfully simulated an ensemble of short-chains of SPIOs using a computational model of magnetic dipole-coupled Langevin saturators. The model accurately predicts hysteresis, and also predicts the experimentally measured order-of-magnitude improvements in SNR and spatial resolution. These findings will be crucial for practical SFMIO synthesis and FDA safety. Indeed, the primary value of the simulation is to estimate uniformity constraints on chain length and shell coating thickness for SFMIO behavior.

Acknowledgments

Funding: The authors acknowledge support from NIH grants R01s EB019458, EB024578, EB029822 and R44: EB029877, UC TRDRP grant 26IP0049, M. Cook Chair, Bakar Fellowship, UC Discovery Award, UCB Bioengineering Craven Fellowship, NSERC PGSD3-532656-2019 fellowship.

Author's statement

Conflict of interest: S. M. C. is a co-founder of an MPI company, Magnetic Insight, and holds stock in this company. The authors declare no other conflict of interest.

References

[1] B. Gleich and J. Weizenecker. Tomographic imaging using the nonlinear response of magnetic particles. *Nature*, 435(7046):1214–1217, 2005, doi:10.1038/nature03808.

[2] X. Zhou, P. Chandrasekharan, D. Mai, K. Jeffris, E. Yu, B. Zheng, and S. Conolly. White blood cell tracking with magnetic particle imaging. *IWMPI*, 2019.

[3] B. Zheng, P. Marc, E. Yu, B. Gunel, K. Lu, T. Vazin, D. V. Schaffer, P. W. Goodwill, and S. M. Conolly. Quantitative magnetic particle imaging monitors the transplantation, biodistribution, and clearance of stem cells in vivo. *Theranostics*, 6(3):291, 2016, doi:10.7150/thno.13728.

[4] E. Y. Yu, P. Chandrasekharan, R. Berzon, Z. W. Tay, X. Y. Zhou, A. P. Khandhar, R. M. Ferguson, S. J. Kemp, B. Zheng, P. W. Goodwill, *et al.* Magnetic particle imaging for highly sensitive, quantitative, and safe in vivo gut bleed detection in a murine model. *ACS nano*, 11(12):12067–12076, 2017, doi:10.1021/acsnano.7b04844.

[5] X. Y. Zhou, K. E. Jeffris, Y. Y. Elaine, B. Zheng, P. W. Goodwill, P. Nahid, and S. M. Conolly. First in vivo magnetic particle imaging of lung perfusion in rats. *Physics in Medicine & Biology*, 62(9):3510, 2017, doi:10.1088/1361-6560/aa616c.

[6] P. W. Goodwill and S. M. Conolly. The x-space formulation of the magnetic particle imaging process: 1-d signal, resolution, bandwidth, snr, sar, and magnetostimulation. *IEEE transactions on medical imaging*, 29(11):1851–1859, 2010, doi:10.1109/TMI.2010.2052284.

[7] J. Rahmer, J. Weizenecker, B. Gleich, and J. Borgert. Signal encoding in magnetic particle imaging: Properties of the system function. *BMC medical imaging*, 9(1):1–21, 2009, doi:10.1186/1471-2342-9-4.

[8] P. W. Goodwill, J. J. Konkle, B. Zheng, E. U. Saritas, and S. M. Conolly. Projection x-space magnetic particle imaging. *IEEE transactions on medical imaging*, 31(5):1076–1085, 2012, doi:10.1109/TMI.2012.2185247.

[9] Z. W. Tay, S. Savliwala, D. W. Hensley, K. B. Fung, C. Colson, B. D. Fellows, X. Zhou, Q. Huynh, Y. Lu, B. Zheng, *et al.* Superferromagnetic nanoparticles enable order-of-magnitude resolution & sensitivity gain in magnetic particle imaging. *Small Methods*, pp. 2100796, doi:10.1002/smtd.202100796.

[10] D. G. Rancourt. 7. magnetism of earth, planetary, and environmental nanomaterials. *Nanoparticles and the Environment*, pp. 217–292, 2018, doi:10.2138/rmg.2001.44.07.

